K-Band High-Power Single-Tuned IMPATT Oscillator Stabilized by Hybrid-Coupled Cavities

YUKIO ITO, HIDEMITSU KOMIZO, TAKESHI MEGURO, MASAICHI SHINODA, TOSHIO OYA, AND YOSHIMASA DAIDO

Abstract—A *K*-band high-power and highly stable power source has been developed using a cavity-stabilized IMPATT-diode oscillator followed by a one-stage high-power reflection-type IMPATT-diode amplifier. The power source shows an output power of 0.7 W, a temperature coefficient of 6×10^{-7}/°C, and an FM noise level of 92-Hz rms/1-kHz $\overline{BW}$ at 100 kHz from the carrier.

To achieve a highly stable oscillation, free from mode jumping, a new hybrid-coupled cavity circuit with a passivating absorber is applied to stabilize the oscillation. The high-power amplifier is designed using a measured large signal device admittance and a power-adding concept.

I. Introduction

MANY AUTHORS have studied cavity-stabilizing methods without a passivating circuit to obtain a highly stable and low-noise Gunn- or IMPATT-diode oscillator [1], [2]. However, in the frequency range beyond the *K* band, the parasitic elements of the diode package greatly influence the circuit impedance, and it becomes rather difficult to obtain a reproducible and tunable stabilized oscillator by such a stabilizing method. Recently, Kohiyama proposed a band rejection-type stabilizing method that allows a single-tuned (i.e., free from mode jump) oscillator [3].

In this paper, a new stabilized oscillator using hybrid-coupled high-*Q* cavities is demonstrated. The resulting circuit provides a highly stable IMPATT-diode oscillator with low power dissipation in the *K* band.

The large signal operation of an IMPATT-diode amplifier was discussed in previous papers [4]–[6]. However, these papers did not describe the detail of the saturation effect, which produces a maximum available generated power from a diode. The authors have verified the saturation effect of the IMPATT diode, using the measured electronic admittance. The developed *K*-band IMPATT-diode amplifier shows an excellent temperature performance with a high output power, and very stable amplification. Furthermore, to eliminate an unstable phenomena observed under large signal conditions, the stabilizing circuit [7] for the passivation of out-of-band oscillations has been applied to the IMPATT-diode mount of the oscillator and amplifier.

Combining the cavity-stabilized IMPATT-diode oscillator and the one-stage IMPATT-diode amplifier, a *K*-band high-power and highly stable power source has been developed.

Manuscript received May 30, 1972; revised August 16, 1972. This paper was presented at the 1972 International Microwave Symposium, Chicago, Ill., May 22–24, 1972.

Y. Ito, H. Komizo, T. Meguro, T. Oya, and Y. Daido are with the Radio Transmission Laboratory, Fujitsu Laboratories, Ltd., No. 1015 Kamikodanaka, Nakahara-Ku, Kawasaki, Japan 211.

M. Shinoda is with the Semiconductor Laboratory, Fujitsu Laboratories, Ltd., No. 1015 Kamikodanaka, Nakahara-Ku, Kawasaki, Japan 211.

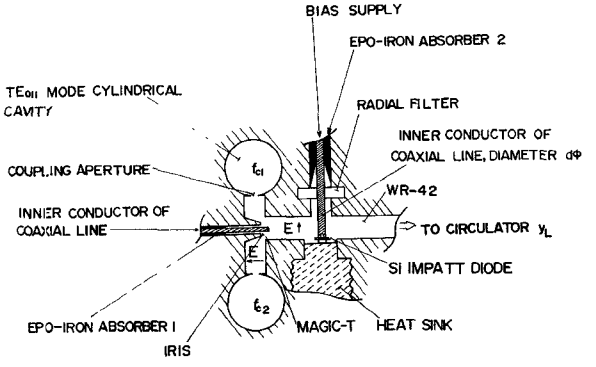

Fig. 1. Cross-sectional view of the cavity-stabilized IMPATT oscillator stabilized by hybrid-coupled cavities.

II. Synthesis of Cavity-Stabilized Oscillator

A hybrid-coupled cavity construction is known as a part of a microwave discriminating circuit that has a high external Q (Q_{ex}), i.e., high-frequency sensitivity, and also roughly a single tuned admittance locus. The proposed solid-state oscillator stabilized by the hybrid-coupled cavities provided a single-mode oscillation without mode jumping, a broad-band mechanical tunability, and higher external Q.

Fig. 1 shows a cross-sectional view of the cavity-stabilized IMPATT oscillator (CSIO) stabilized by hybrid-coupled cavities (HCC). Two TE_{011}-mode high-Q cavities, with resonant frequencies of f_{c1} and f_{c2}, are connected to both arms of the *H* plane T junction through the coupling apertures. The coaxial arm is terminated with an Epo–iron (mixture of Epoxy–plastic and Carbonyle–iron powder) absorber 1. A reduced-height pill-type packaged Si IMPATT diode is mounted in the coaxial line, which is extended from the WR-42 waveguide. At the other side of the coaxial line, the stabilizing and the biasing circuit are provided. The stabilizing circuits consist of a radial filter and an Epo–iron absorber 2, which

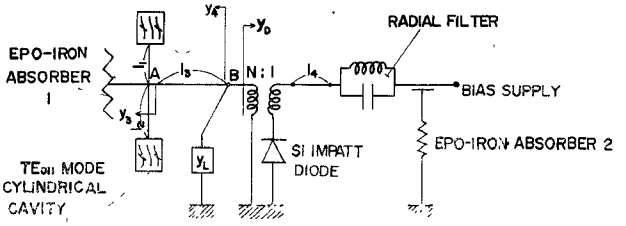

Fig. 2. Simplified equivalent circuit of the stabilized oscillator, y_3, y_4, and y_D are normalized by waveguide admittance Y_0.

play an important role in restraining out-of-band spurious oscillations. The coaxial post diameter $D\phi$ of the coaxial inner conductor mainly determines the coupling between the diode and the waveguide circuit [8], [9].

Fig. 2 shows a simplified equivalent circuit of the stabilized oscillator. The distance from the center of the magic-T to each cavity are l_1 and l_2, respectively, and the difference l_2-l_1 is chosen as nearly $(2n-1)\lambda_{gc}/4$, where λ_{gc} is the wavelength in the waveguide of the center frequency f_c, and $f_c=(f_{c1}+f_{c2})/2$. Therefore, the normalized admittance of the HCC, looking from point A, is roughly matched to the waveguide impedance, in the out-of-band frequency region.

Assuming an ideal magic-T and a lossless line, the normalized admittance y_4 at the diode-post position, looking from point B, separated from point A by a distance of l_3, is given as follows:

$$y_4 = \frac{1-\Gamma_4}{1+\Gamma_4} = g_4 + jb_4 \tag{1}$$

where Γ_4 is the reflection coefficient of the HCC at point B,

$$\begin{aligned}\Gamma_4 &= \Gamma_3 e^{-j2\beta l_3} \\ &= \frac{1}{2}\left\{\frac{1-(g_1+j\Omega_1)}{1+(g_1+j\Omega_1)} e^{-j2\beta l_1} + \frac{1-(g_2+j\Omega_2)}{1+(g_2+j\Omega_2)} e^{-j2\beta l_2}\right\} e^{-j2\beta l_3} \qquad (2)\\ g_1 &= Q_{e1}/Q_{01} \\ g_2 &= Q_{e2}/Q_{02} \\ \Omega_1 &= Q_{e1}(\omega/\omega_{c1} - \omega_{c1}/\omega) \\ \Omega_2 &= Q_{e2}(\omega/\omega_{c2} - \omega_{c2}/\omega)\end{aligned}$$

Q_{e1}, Q_{e2} external Q of each cavity;
Q_{01}, Q_{02} unloaded Q of each cavity;
ω_{c1}, ω_{c2} resonant angular frequencies of each cavity;
β phase constant $(=2\pi/\lambda_g)$.

In the case of $f_{c1}>f_{c2}$, $l_1=\lambda_{gc}/8$, $l_2=l_1+\lambda_{gc}/4$, $Q_{e1}=Q_{e2}=2500$, and $Q_{01}=Q_{02}=15\,000$, y_4 loci can be calculated as parameters of $\Delta f_c/f_c$, using (2) as shown in Fig. 3, where $\Delta f_c=f_{c1}-f_{c2}$. These loci behave like that of a staggered tuned band rejection filter. Length l_3 is so chosen as to satisfy the oscillating condition. In this calculation, the diode susceptance is assumed to be zero at a normal operating condition.

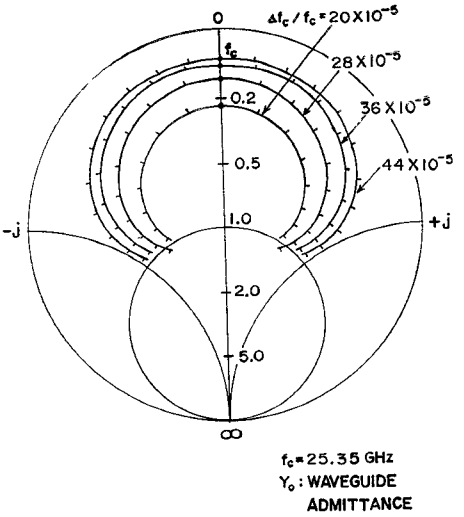

Fig. 3. Calculated input admittance y_4 loci of the HCC looking from point B in Fig. 2, as a parameter of $\Delta f_c/f_c$ where the markers on the loci indicate 1-MHz spaced frequencies, $Q_{01}(=Q_{02})=15\,000$, $Q_{e1}(=Q_{e2})=2500$, and $f_c=25.35$ GHz.

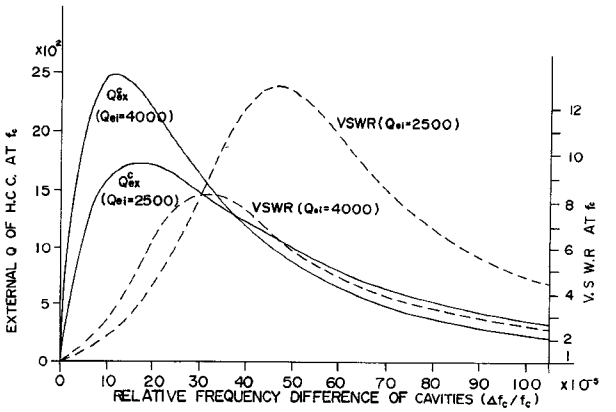

Fig. 4. Calculated external Q and VSWR of HCC versus the relative frequency difference $\Delta f_c/f_c$, where $Q_0=15\,000$, and $f_c=25.35$ GHz.

The external Q of the HCC $(=Q_{ex}{}^c)$ at the center frequency f_c and the bandwidth of the band rejection filter are a function of the Q_{ei} of each cavity and the frequency difference Δf_c. The $Q_{ex}{}^c$ and VSWR at the center frequency f_c are given by

$$Q_{ex}{}^c = \frac{\omega}{2}\frac{\partial}{\partial\omega}\left(\frac{B_4}{Y_0}\right) = \frac{\omega}{2}\frac{\partial b_4}{\partial\omega}\bigg|_{\omega=\omega_c} \tag{3}$$

$$\text{VSWR} = \frac{1+|\Gamma_4|}{1-|\Gamma_4|}. \tag{4}$$

Fig. 4 shows the calculated $Q_{ex}{}^c$ and VSWR values at f_c versus relative frequency difference $\Delta f_c/f_c$. At the given Q_{ei} and Q_0, there are a maximum $Q_{ex}{}^c$ and a maximum VSWR at specific $\Delta f_c/f_c$ values, respectively. The values of $Q_{ex}{}^c$ and VSWR approximately determine the frequency stability and output power. At point B in Fig. 2, the normalized output load admittance y_L and diode admittance y_D are connected to y_4 in parallel.

When the unstabilized oscillating frequency ω_0 changes to ω_0' due to the variation of temperature or

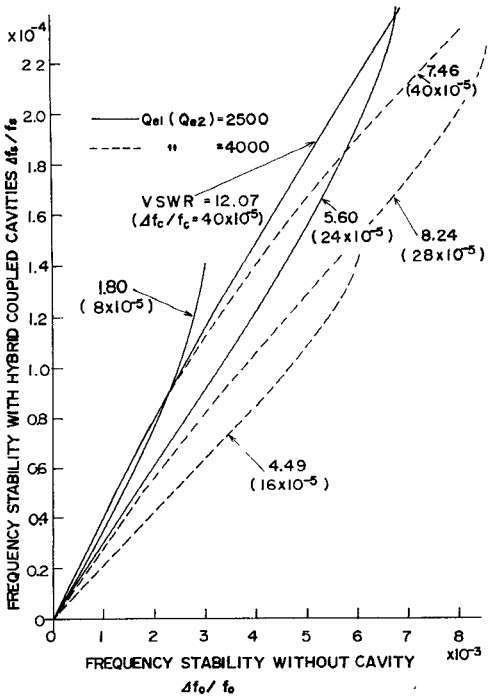

Fig. 5. Calculated frequency stability of the stabilized oscillator $\Delta f_s/f_s$ versus the unstabilized frequency stability $\Delta f_0/f_0$ with $\Delta f_c/f_c$ as parameters, where $Q_0=15\ 000$, $Q_1=50$, and $f_c=25.35$ GHz.

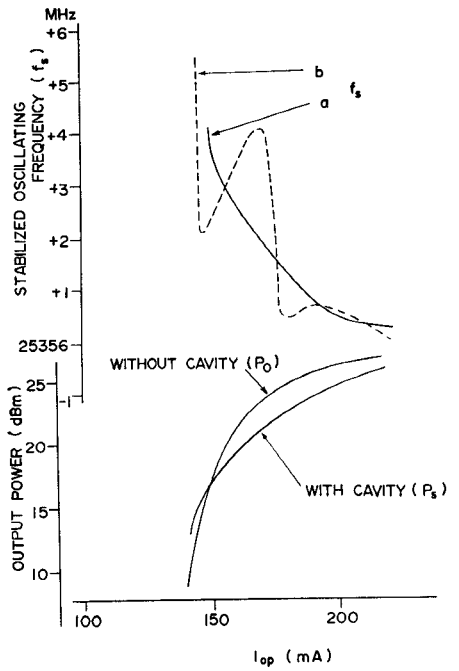

Fig. 6. Typical oscillating characteristics of the cavity-stabilized IMPATT oscillator at room temperature, where $Q_0=15\ 000$, $Q_{ei}=2500$, $\Delta f_c=10$ MHz, and $Q_1=50$, and curves *a* and *b* correspond to different dimensional combinations in the mount.

biasing conditions, the susceptance of unstabilized oscillator $\Delta b(\omega)$ is given by

$$\Delta b(\omega) = Q_1(\omega/\omega_0' - \omega_0'/\omega) \tag{5}$$

where Q_1 is the external Q of the unstabilized oscillator, $\omega_0'=\omega_0\pm\Delta\omega_0$.

Then the circuit susceptances of the cavity-stabilized oscillator must satisfy the following equations at the oscillating frequency ω_s,

$$\Delta b(\omega_s) + b_4(\omega_s) = 0 \tag{6}$$

$$\left.\frac{\partial\{\Delta b(\omega) + b_4(\omega)\}}{\partial\omega}\right|_{\omega=\omega_s} \tag{7}$$

where $\omega_s=\omega_0\pm\Delta\omega_s$ and $\Delta\omega_s$ is the frequency difference between ω_0 and ω_s.

Fig. 5 shows the calculated frequency stability of the oscillator with high-Q cavities with Q_{ei} values of 2500 and 4000, respectively, and VSWR as a parameter at a center frequency f_c versus the frequency stability of the unstabilized oscillator with Q_1 of 50. From Figs. 5 and 4, the frequency stabilities $\Delta f_s/f_s$ with hybrid-coupled cavities become approximately minimum at the relative frequency differences $\Delta f_c/f_c$, which give the maximum $Q_{ex}{}^e$ values.

The power loss of the oscillator due to the HCC is given by the following equation.

$$\text{power loss} = 10\log\left(\frac{\text{VSWR}}{1+\text{VSWR}}\right)^2. \tag{8}$$

The above equation is derived using the following assumption; the diode operates at the same negative conductance point in both the stabilized and unstabilized conditions.

III. Cavity-Stabilized IMPATT Oscillator

The Si IMPATT diode (made by Fujitsu Laboratories, Ltd.) used for the oscillator and the amplifier has about a 10^{-4}-cm^2 junction area, a thermal resistance of below 16°C/W, a breakdown voltage of 40 V, and an avalanche frequency of about 13 GHz when operating current $I_{op}=210$ mA. The diode is soldered to a copper block for a good heat sink of about 2.5°C/W thermal resistance. Typical output power and efficiency are about 26.5 dBm and 4.3 percent, with a junction temperature of 230°C.

Fig. 6 shows typical oscillating characteristics of the stabilized IMPATT oscillator mentioned above. In this experiment, the following values were chosen for the parameters; $Q_{01}=Q_{02}=15\ 000$, $Q_{e1}=Q_{e2}=2500$, $Q_1=50$, and $\Delta f_c=10$ MHz. The solid lines show the performances of the normal adjusted oscillator. However, when length l_4 and other circuit parameters are changed to some combination, the oscillating frequency derivative Δf_s, with the operating current deviation ΔI_{op}, becomes positive in some regions of I_{op}, as shown in Fig. 6. This indicates that the oscillating frequency of the original oscillator (without cavity) can be changed to various temperature coefficient (TC) values from negative to positive, according to the circuit's parameters.

In this case, the calculated $Q_{ex}{}^e$, VSWR, and power loss are about 1200, 12, and 0.75 dB, respectively. From the measured electronic admittance, the available out-

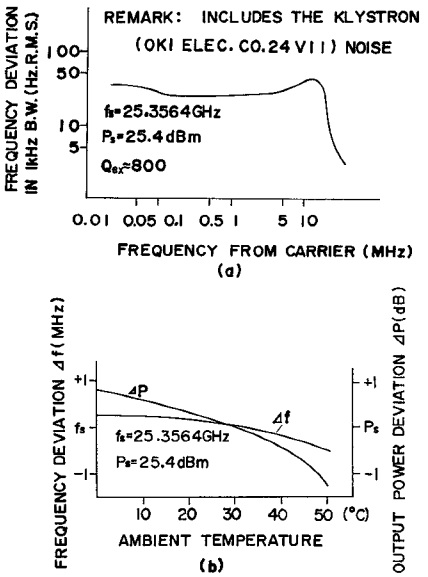

Fig. 7. (a) FM noise characteristic of CSIO using HCC of Fig. 6. (b) Oscillating frequency and output power deviation versus an ambient temperature of CSIO using HCC of Fig. 6.

put power P_o of this oscillator without cavities is about 26.5 dBm. Therefore, the calculated output power of the stabilized oscillator becomes 25.75 dBm. However, a stabilized output power P_s of about 25.4 dBm was obtained at 25.35 GHz with a pushing figure of 17.5 kHz/mA and an efficiency of 3.3 percent at the operating junction temperature of 230°C. The external Q of this oscillator ($=Q_{ex}$) is about 800, which is derived from the measured injection-locked bandwidth.

Fig. 7(a) shows typical FM noise characteristics, using the CSIO of Fig. 6. The FM noise is about 38-Hz rms in 1-kHz $\overline{BW}$ at 100 kHz from the carrier, as shown in Fig. 7(a), which includes the noise of the measurement klystron. The cavities are made of an alloy of Invar ($TC=1\sim2\times10^{-6}$/°C). Its inner diameter is 18.1 mm. The CSIO without temperature compensation for the cavities has a frequency stability $\Delta f_s/f_s$ of 1.1×10^{-4}/40°C (i.e., 2.75×10^{-6}/°C). On the other hand, the frequency stability of the unstabilized oscillator $\Delta f_o/f_o$ shows 1.1×10^{-3}/40°C (i.e., 2.75×10^{-5}/°C).

From the theoretical calculation of Fig. 5, the $\Delta f_s/f_s$ of 1.1×10^{-4} corresponds to the $\Delta f_o/f_o$ of 2.8×10^{-3} from the curve of VSWR 12.07 and $Q_{ei}=2500$. The difference between both $\Delta f_o/f_o$ values is about a factor of two. The reason for this difference appears to be that the IMPATT-diode mounts for the CSIO, and that for the unstabilized oscillator, have different external Q_1 values, due to different adjustment to obtain the maximum available oscillating power, respectively. Adopting a temperature compensation using a copper short plunger and a simple humidity protection of the CSIO cavities [1, p. 891, Fig. 1(b)], the resultant relative frequency deviation can be reduced to the order of 10^{-7}/°C. Fig. 7(b) shows the frequency and power deviations versus temperature, using the temperature compensated CSIO of Fig. 6. Resultant relative frequency deviation of less than $3\times10^{-5}/0\sim50$°C and output power variation of less than 2 dB/0~50°C at $P_s=25.4$ dBm have been obtained. The principle of this stabilization scheme has been also applied, with very good operating results, to the highly stable Gunn-diode oscillators in the range from 15 to 25 GHz. The 15 GHz and 25 GHz highly stable Gunn-diode oscillators showed relative frequency deviations of less than $4\times10^{-5}/-10\sim+50$°C, with output power deviations of less than 1.5 dB/$-10\sim+50$°C at the nominal output power of about 20 dBm, respectively.

IV. Amplifier and Resultant Power Source

The amplifier diode mount is almost the same construction as that shown in Figs. 1 and 2, except for the HCC being replaced by a short plunger. The center operating frequency of amplifier can be roughly tuned by l_4 and the gain roughly adjusted by l_3. The stabilizing circuit with an absorber 2 eliminates unstable nonlinear phenomena. Fig. 8 shows a circuit diagram of the reflection-type amplifiers. The diode at port 2–2′ is connected to port 1–1′ of the circulator through matching network M. Output power P_{out} of an amplifier is roughly the sum of input power P_{in} and generated power P_g.

For a better understanding of the amplifier nonlinearity, electronic admittance of the IMPATT diode was measured using reflection gain and phase (see the Appendix). The IMPATT diode is divided into two parts for treatment convenience. One is the active layer of the IMPATT diode and the other is the passive region, which contains the contact resistance and the resistance of the substrate. This latter one is included in network M. Therefore, electronic admittance $\overline{Y}_D$ is the admittance of the active layer only. Fig. 9 shows the results of the measured electronic admittance and the generated power at two different ambient temperatures versus RF voltage. The electronic conductance is sharply reduced at an RF voltage of about 18 V. This causes a rapid drop of the amplifier gain at the corresponding input level. The maximum generated power of this diode, excluding the series resistance, is estimated at about 1.5 W. This power reduced to 650 mW due to the 1.3-Ω series resistance. The series resistance is measured by the method in [10]. Using this diode in the oscillator, an actual available power $P_{g\,av}$ of 450 mW was obtained in the present experiment. Therefore, the difference power of 200 mW seems to be lost in the circuit. The temperature dependence of $\overline{Y}_D$ is within the measurement error range. Fig. 10 shows the saturation characteristics of the amplifier designed for small signal gain values G_s of 5 and 8 dB at various ambient temperatures. When $G_s=8$ dB, the saturation and the gain expansion occur in the small input level, and 1-dB gain compression input level is about 19 dBm. For the K-band IMPATT power source, the small signal gain of the amplifier was designed at 5 dB. When $G_s=5$ dB, the output power gradually saturates up to about a 25-dBm input level, and 1-dB gain compression input level is about 23 dBm. The output changes near the input power of about 27 dBm, and increasing of the saturation

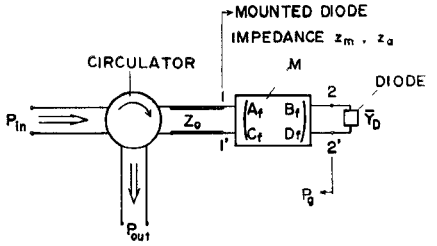

Fig. 8. Reflection-type amplifier circuit diagram.

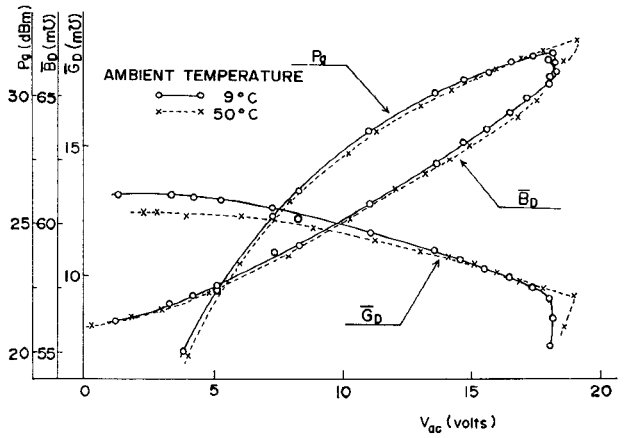

Fig. 9. RF voltage dependency of electronic admittance $\overline{Y}_D$ and generated power P_g from the diode.

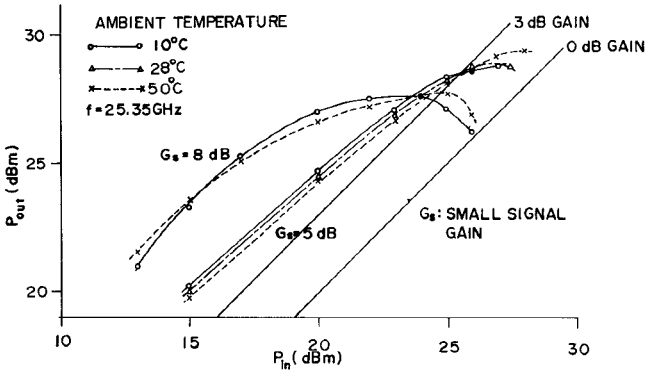

Fig. 10. Saturation characteristics of *K*-band IMPATT amplifier at various ambient temperatures.

power at 50°C depends on the temperature dependency of $\overline{Y}_D$ and the load admittance. At a P_{in} of about 26 dBm, P_{out} is almost independent of the ambient temperature variation. Since the input power from CSIO is from 24.2~26.2 dBm, the output power from the amplifier shows 27.6~28.7 dBm with a gain of about 3 dB over the temperature range of 0 to 50°C. The 1-dB bandwidth is about 3 GHz at a P_{in} of 25 dBm and a gain of about 3 dB. The noise figure is 35.3 dB under an operating current of 166 mA. This value changes to 37.6 dB and 33.3 dB at the other operating currents of 200 mA and 100 mA, respectively. A block diagram and photograph of *K*-band power source are shown in Fig. 11. The two silica-gel capsules are mounted on the end-plate side of the cavities. Due to the O-rings at the contact planes and the Mylar windows, the cavities are almost entirely isolated from external atmosphere.

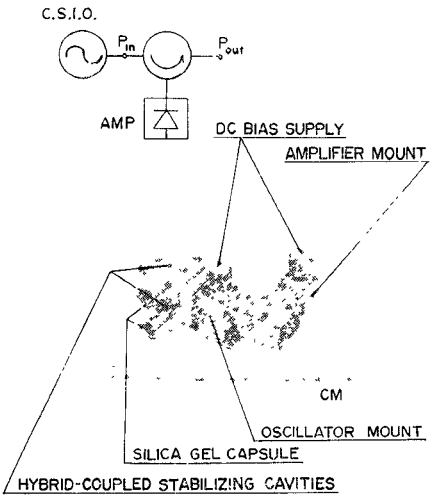

Fig. 11. Block diagram and photograph of the *K*-band high-power highly stable IMPATT power source.

Overall performance shows an output power of more than 580 mW within the frequency deviation of about 3×10^{-5} over the ambient temperature of 0~50°C. The overall FM noise is 92-Hz rms/1-kHz $\overline{BW}$ at 100 kHz from a carrier at about 28-dBm output level, including the FM noise of 38-Hz rms from the CSIO. The overall FM noise at the 10-dBm amplifier input level nearly coincides with the FM noise of CSIO (i.e., 38-Hz rms).

V. Conclusion

The new cavity-stabilizing oscillator demonstrated here has many advantages, such as a single-mode oscillation, a high external Q over a wide-temperature range, and ease of design. This method can be applied to a higher frequency range than *K* band. Also the study of the large-signal IMPATT-diode admittance, measured by a new circuit parameter method, well supports the design of the amplifier and understanding of its nonlinearity. The resultant *K*-band power source has shown a frequency temperature coefficient of 6×10^{-7}/°C and an output power of about 700 mW, with a moderate junction temperature of 230°C.

This power source is suitable for a stable and reliable local oscillator for millimeter-wave PCM systems, and for pumping source of a parametric amplifier.

Appendix

Measurement of Large Signal IMPATT Admittance

A. Determination of Network Parameters

When the bias voltage of the diode is smaller than breakdown voltage V_B, impedance Z_d of the active layer of an IMPATT diode is given by (9)

$$Z_d(V) = r(V) - j(1/\omega C_d(V)) = r(V) - jX_d(V) \quad (9)$$

where $r(V)$ and $C_d(V)$ are the resistance of the unswept region and the bias voltage dependent capacitance, respectively. $r(V)$ and $C_d(V)$ have the following relation.

$$r(V) = W/(\sigma A) - \epsilon/(\sigma C_d(V)) \tag{10}$$

where W, A, σ, and ϵ are width, junction area, conductivity, and dielectric constant of the n layer, respectively. The fundamental parameters of network M in Fig. 8 are denoted as A_f, B_f, C_f, and D_f. The circulator characteristic impedance is denoted as Z_0. Then the necessary circuit parameters are determined by measuring normalized mounted-diode impedance z_m, looking from the 1–1′ plane to the diode side as a function of C_d. Then z_m is given as follows:

$$z_m = \frac{A_f Z_d + B_f}{Z_0(C_f Z_d + D_f)} = \frac{aZ_d + b}{cZ_d + 1} = r_m + jx_m \tag{11}$$

where

$$\begin{aligned} a &= A_f/(Z_0 D_f) \\ b &= B_f/(Z_0 D_f) \\ c &= C_f/D_f \\ 1 &= A_f D_f - C_f B_f = Z_0 D_f^2(a - bc). \end{aligned} \tag{12}$$

a, b, and c can be determined from measured impedance z_m by the least-square approximation as follows. First, measured impedance z_m values are approximated with the polynomial of X_d, using the principle of least square. Z_d can be shown as a function of X_d using (9) and (10). This Z_d is substituted into (11), and the resulting equation is expanded as the power series of X_d. Then two X_d polynomials are given which must both express the same quantity z_m. The first 3 lower coefficients of X_d in one polynomial are equated with the coefficients of the same order of X_d in the other polynomial. Then the equations which determine a, b, and c are derived. Using the thus determined a, b, and c, the higher order coefficients of X_d in one polynomial may not coincide with the same order coefficients of X_d in the other one. Therefore, the reference-plane position with which the power series of X_d converges most rapidly was chosen. In this case, the calculation error caused by the disagreement of higher order coefficients of X_d are smaller than 1 percent throughout the full variation range of X_d. Fig. 12 shows the normalized resistance r_m and reactance x_m versus the junction reactance X_d curves. From this figure, it can be seen that the measured points closely coincide with the calculated curves, within a 10-percent error.

B. Determination of Electronic Admittance

When the bias voltage becomes larger than V_B, the diode shows an admittance $\overline{Y}_D$ with a negative real part, and the circuit of Fig. 8 can be operated as a reflection-type amplifier. The normalized mounted-diode impedance z_a can be measured as a function of input RF signal levels. Then the electronic admittance $\overline{Y}_D$ can be easily obtained, using normalized impedance z_a with a negative real part and network parameters a, b, and c.

$$\begin{aligned} z_a &= (1 + \Gamma)/(1 - \Gamma) = (a + b\overline{Y}_D)/(c + \overline{Y}_D) \\ \overline{Y}_D &= (cz_a - a)/(b - z_a) = -\overline{G}_D + j\overline{B}_D \end{aligned} \tag{13}$$

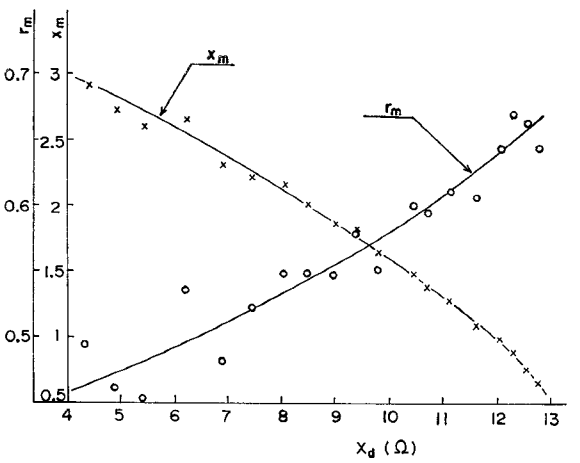

Fig. 12. Normalized diode mount resistance r_m and reactance x_m versus the junction reactance X_d. When bias voltage $< V_s$, cross and circle points and the solid lines indicate the measured results and calculated least-square approximation curves, respectively.

where Γ is the complex reflection coefficient whose modulus is greater than one, and $|\Gamma|^2 = P_{out}/P_{in}$. The RF voltage V_{ac} applied to $\overline{Y}_D$ and P_g can be calculated as follows. Using the boundary condition at 1–1′ plane and the definition of F parameters, we can easily derive the following equation:

$$\begin{aligned} V_+ &= \frac{1}{2}(D_f Z_0 + B_f)\left(\frac{A_f + Z_0 C_f}{D_f Z_0 + B_f} + \overline{Y}_D\right) V_{ac} \\ &= \frac{1}{2} D_f Z_0 (b + 1)\left(\frac{a + c}{b + 1} + \overline{Y}_D\right) V_{ac} \\ P_{in} &= \frac{1}{2}\frac{|V_+|^2}{Z_0} \\ &= \frac{1}{8} Z_0 |D_f|^2 |(b + 1)\overline{Y}_D + a + c|^2 V_{ac}^2 \end{aligned} \tag{14}$$

where V_+ is voltage incident wave at 1–1′ plane. Substituting the last equation in (12) into (14), V_{ac} is obtained.

$$\begin{aligned} V_{ac} &= (8|a - bc|P_{in})^{1/2}/|a + c + (b + 1)\overline{Y}_D| \\ P_g &= \tfrac{1}{2}\overline{G}_D V_{ac}^2. \end{aligned} \tag{15}$$

Using (13) and (15), $\overline{Y}_D$, V_{ac}, P_g are calculated. Results are shown in Fig. 9.

Acknowledgment

The authors wish to thank Dr. Kojima, Managing Director, F. Iwai and Dr. H. Yunoki, Managers of the Radio Transmission Laboratory, Dr. T. Oshida, Dr. T. Misugi, and Dr. Y. Hukukawa, Managers of the Semiconductor Laboratory, Fujitsu Laboratories, Ltd., for their encouragement during this study; H. Takanashi and M. Yamamoto, for their development of diodes, and S. Masuda, F. Mita, and Y. Shimoji for their helpful discussion and experimental cooperation.

References

[1] Y. Ito, H. Komizo, and S. Sasagawa, "Cavity stabilized X-band Gunn oscillator," *IEEE Trans. Microwave Theory Tech. (Special*

Issue on Microwave Circuit Aspects of Avalanche-Diode and Transferred Electron Devices), vol. MTT-18, pp. 890–897, Nov. 1970.
[2] S. Nagano and H. Kondo, "Highly stabilized half-watt IMPATT oscillator," *IEEE Trans. Microwave Theory Tech. (Special Issue on Microwave Circuit Aspects of Avalanche-Diode and Transferred Electron Devices)*, vol. MTT-18, pp. 885–890, Nov. 1970.
[3] K. Kohiyama and K. Momma, "A new type of frequency-stabilized Gunn oscillator," *Proc. IEEE* (Corresp.), vol. 59, pp. 1532–1533, Oct. 1971.
[4] E. F. Scherer, "Large-signal operation of avalanche-diode amplifiers," *IEEE Trans. Microwave Theory Tech. (Special Issue on Microwave Circuit Aspects of Avalanche-Diode and Transferred Electron Devices)*, vol. MTT-18, pp. 922–932, Nov. 1970.
[5] C. W. Lee and W. C. Tsai, "High power GaAs avalanche diode amplifiers," in *IEEE Int. Conv., Dig. Tech. Papers*, Mar 1971, pp. 368–369.
[6] M. E. Hines, "Special problems in IMPATT diode power amplifiers," in *1972 IEEE Int. Solid-State Circuits Conf. Tech. Papers*, Feb. 1972, pp. 34–35.
[7] H. Komizo, Y. Ito, H. Ashida, and M. Shinoda, "A 0.5-W CW IMPATT amplifier for high-capacity 11 GHz radio-relay equipment," in *1972 IEEE Int. Solid-State Circuits Conf. Dig. Tech. Papers*, Feb. 1972, pp. 36–37.
[8] W. C. Tsai, F. J. Rosenbaum, and L. A. MacKenzie, "Circuit analysis of waveguide-cavity Gunn-effect oscillator," *IEEE Trans. Microwave Theory Tech. (Special Issue on Microwave Circuit Aspects of Avalanche-Diode and Transferred Electron Devices)*, vol. MTT-18, pp. 808–817, Nov. 1970.
[9] D. C. Hanson and J. E. Rowe, "Microwave circuit characteristics of bulk GaAs oscillator," *IEEE Trans. Electron Devices (Second Special Issue on Semiconductor Bulk Effect and Transit-Time Devices)*, vol. ED-14, pp. 469–476, Sept. 1967.
[10] E. W. Sard, "A new procedure for calculating varactor Q from impedance versus bias measurements," *IEEE Trans. Microwave Theory Tech.*, vol. MTT-16, pp. 849–860, Oct. 1968.
[11] J. W. Gewartowski and J. E. Morris, "Active IMPATT diode parameters obtained by computer reduction of experimental data," *IEEE Trans. Microwave Theory Tech.*, vol. MTT-18, pp. 157–161, Mar. 1970.

Intermodulation Characteristics of X-Band IMPATT Amplifiers

ROBERT J. TREW, NINO A. MASNARI, AND GEORGE I. HADDAD

Abstract—**The intermodulation products produced when two equal-amplitude signals are applied to the input of an X-band IMPATT-diode amplifier have been measured. An Si p^+nn^+ IMPATT diode was operated in a double-slug-tuned coaxial reflection amplifier circuit that was tuned to provide 20 dB of small-signal gain at 9.340 GHz. The intermodulation tests consist of measurements of the magnitudes and frequencies of the amplifier output signals as a function of the input-signal drive levels and frequency separations. The gain and single-frequency characteristics of the amplifier were also measured, and are used along with the theoretical device and circuit admittance characteristics as a basis for explanation of the intermodulation results. A low-frequency dominance mechanism is found to exist in which the low-frequency signals are amplified more than the high-frequency signals. This mechanism becomes more significant as the amplifier drive level is increased.**

Introduction

As a result of the inherent nonlinearity associated with large-signal operation of avalanche transit-time devices [1], the introduction of two or more nonharmonically related signals into the input of an IMPATT amplifier results in the generation of intermodulation signals in the amplifier output. The distortion mechanism resulting from the production of these signals reduces the available power levels at the amplifier fundamental frequencies [2]. Measurements have been made of the intermodulation products generated when two equal-amplitude signals are applied to the input of an X-band IMPATT-diode amplifier.

The test results consist of measurements of amplifier output signals as a function of input-signal power levels and frequency separations. The results presented are typical for IMPATT-diode amplifiers. In particular, diodes fabricated at the Electron Physics Laboratory of the University of Michigan, as well as commercially available diodes, were tested and yielded similar results. Use is made of the IMPATT device and circuit admittance characteristics to explain the output behavior of the amplifier.

Circuit Description

The block diagram of Fig. 1 represents the basic reflection amplifier circuit used in these experiments. Input–output signal separation is provided by a coaxial three-port circulator. Amplifier tuning is accomplished through the positioning in the resonant cavity of two 20-Ω copper tuning slugs; one being $\lambda/4$ at 8 GHz, the other $\lambda/4$ at 10 GHz. The diode is located at the end of the resonant cavity and is kept at an approximately constant temperature by a water-cooled heat sink. The two source signals are amplified for large-signal operation and are introduced into the amplifier input through a "magic-T" that insures source signal isolation. The primary measurement circuit consists of a precision

Manuscript received April 28, 1972; revised August 16, 1972. This work was supported by the National Aeronautics and Space Administration under Grant NGL 23-005-183. This paper was presented at the 1972 International Microwave Symposium, Chicago, Ill., May 22–24, 1972.

The authors are with the Electron Physics Laboratory, Department of Electrical and Computer Engineering, the University of Michigan, Ann Arbor, Mich. 48104.